AIAA SciTech
13-17 January 2014, National Harbor, Maryland
52nd Aerospace Sciences Meeting

CFD Solver Comparison of Low Mach Flow over the ROBIN Fuselage

Jennifer N. Abras[1]
NAVAIR Applied Aerodynamics and Store Separation Branch, Patuxent River, MD, 20670

and

Nathan Hariharan[2]
CREATE-AV, Lorton, VA, 22079

The ROtor Body INteraction (ROBIN) fuselage is used as a baseline test case for a computational fluid dynamic (CFD) study of solver drag prediction results for low Mach flow. All of the predictions are compared not only to one another, but also to available wind tunnel data. Comparisons of integrated viscous and pressure drag, flow separation point, and centerline pressure distributions are analyzed. Parametric studies of the independent options available within each code for low Mach flow conditions are investigated. Grid studies are also presented. The final comparisons reveal that for the attached flow regions all of the CFD codes predict approximately the same result. The differences occur when the flow begins to separate aft of the fuselage. Benefits are gained when the viscous grid layers are merged from tetrahedrons into prisms, and when the incompressible option is employed. Higher spatial order of accuracy in the separated region is found to slightly improve the results.

I. Introduction

THE CREATE-AV program is focused on developing state-of-the-art software for use with both fixed wing and rotary wing aircraft analysis. These codes are HPCMP CREATE^{TM}-AV HELIOS for rotary wing analysis and HPCMP CREATE^{TM}-AV KESTREL for fixed wing analysis. Release versions of both of these codes are currently in use in government, industry, and academia. However, the development process to expand the capabilities of these codes and to improve on the present capabilities is ongoing. While these changes and improvements encompass a wide range of topics, one specific area of improvement is the addition of a new near-body CFD solver in CREATE-AV HELIOS.

Evaluation of major changes in the configuration of any CFD code are pursued through comparisons to both available measured data as well as to the predictions produced by established CFD solvers. Planned changes to the CREATE-AV HELIOS solver will be evaluated using these types of comparisons. The near-body CFD solver in the current release version of CREATE-AV HELIOS, is NSU3D. Future versions of CREATE-AV HELIOS are planned to transition to the kCFD solver which currently resides in CREATE-AV KESTREL. It is of interest to compare both kCFD and NSU3D to better understand the possible impact that the transition will have on the CREATE-AV HELIOS solver. Predictions from both of these codes will be compared not only to one another, but also to available wind tunnel data and predictions from both the OVERFLOW and FUN3D solvers.

The wind tunnel test case selected for this comparison is centered around the ROBIN-mod7 isolated fuselage. This test was run in the NASA Langley 2 ft x 3 ft wind tunnel. The purpose of this test is to investigate fuselage drag reduction using aft blowing. However, the baseline cases run during this test are suitable for comparison during the present study. Reference 1 contains a subset of the wind tunnel data from this test as well as the OVERFLOW predictions. The outer mold line of this fuselage is defined by a series of equations that are provided in appendix A of reference 1. All test data and OVERFLOW predictions presented herein have been digitized or copied from this paper. Recent CREATE-AV HELIOS evaluations have also used this test data, comparing CREATE-AV HELIOS to a commercial off the shelf (COTS) solver, CFD++[2].

[1] Aerospace Engineer, jennifer.abras@navy.mil, AIAA Professional Member.
[2] Deputy Project Manager, nathan.hariharan.ctr@hpc.mil, AIAA Associate Fellow.

This paper compares the drag predictions of the CREATE-AV HELIOS solver and the CREATE-AV KESTREL solver against available wind tunnel data and predictions made by OVERFLOW and FUN3D. These comparisons include grid density studies, grid boundary layer analysis, incompressible solver evaluation, near-body trim distance analysis, overall solver comparisons, and a timing and convergence comparison. The final comparisons utilize the centerline pressure distributions, center slice velocity contours, flow separation location, and integrated pressure and viscous drag coefficients in order to assess the performance of each code.

II. Methodology

A. HPCMP CREATE™-AV HELIOS v4.0

CREATE-AV HELIOS[3] is a multi-function code designed specifically for rotorcraft analysis. It contains unstructured near-body and Cartesian off-body CFD solvers, overset methodology using PUNDIT, rigid grid motion, and rotor blade structural deformations through RCAS or through prescribed deformations. The near-body solver is NSU3D, a node-centered unstructured CFD code that solves the Reynolds Averaged Navier-Stokes (RANS) equations applying 2nd-order spatial accuracy. The Spalart-Allmaras (SA) and SA-DES turbulence models are available. The unstructured grid can contain a mixture of tetrahedral and prismatic cells. ARC3D is the off-body Cartesian solver which applies up to 5th-order spatial accuracy. This solver may be run inviscid or with the SA-DES turbulence model. This solver also has the option of applying automatic mesh refinement (AMR) to the solution. Cases using NSU3D alone and dual NSU3D and ARC3D are presented. All cases apply the SA turbulence model to the near-body, and the Euler solution in the off-body where applicable. All solutions are run steady-state.

B. HPCMP CREATE™-AV KESTREL v4.0.5

CREATE-AV KESTREL[3] is a multi-function code designed specifically for fixed wing aircraft analysis. It contains a near-body CFD solver (kCFD), control surface motion capability, engine analysis, and 6DoF analysis. kCFD is a cell-centered unstructured CFD code which solves the RANS equation using 2nd-order spatial accuracy. A variety of turbulence models are available including the SA and SA-DDES models. The unstructured grid can contain a mixture of tetrahedral and prismatic cells. This solver also has the option of applying automatic mesh refinement (AMR) to the solution. All cases apply the SA turbulence model and are run steady-state.

C. FUN3D v12.2

The NASA Langley code FUN3D[4] is an unstructured CFD code that solves the RANS equations using a node-centered 2nd-order upwind implicit scheme. The unstructured grid can contain a mixture of tetrahedral and prismatic cells. This code is able to perform a variety of analyses including rigid and elastic grid motion, 6DoF analysis, design optimization, and grid adaptation. This code also contains a variety of rotorcraft specific options including coupling with external comprehensive rotorcraft codes. There are a wide variety of flux schemes and turbulence models available, but for this study the Roe flux scheme and the SA turbulence model have been selected. All cases are run steady-state.

III. Conditions

The wind tunnel model is shown in Figure 1. The model is inverted in order to focus on the flow separation on the lower aft portion of the fuselage. A series of 41 pressure taps are located along the centerline of the fuselage. These pressure taps run along the length of the bottom of the fuselage, and along the top of the fuselage between the nose and the post. The flow conditions utilized include a Mach number of 0.1 (about 34 m/s), a Reynolds number, based on the fuselage length, of 1.6M and an angle of attack of 0°. Standard sea level conditions are assumed in the CFD solutions. The mount shroud is constructed using an extruded NACA0018 airfoil section.

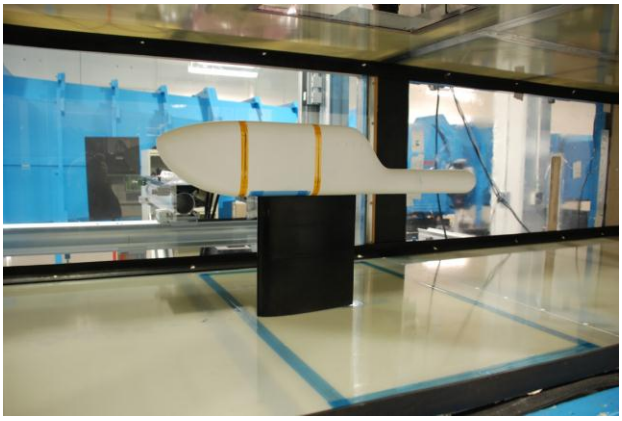

Figure 1. Image of the wind tunnel model from Ref.1.

IV. Grids

The underlying CAD used for this model is in the form of a NASTRAN file. This NASTRAN mesh data was loaded into the Rhinoceros v4.0 CAD program where NURBS surfaces were generated. These NURBS surfaces were used within the NASA Langley TetrUSS tools, GridTool and VGrid, to generate the tetrahedral unstructured grids. All the solvers employed here use unstructured grids, the details for these grids are provided in Table 1. The boundary layers are merged for a majority of the cases. This boundary layer merging is always performed using the CREATE-AV HELIOS preprocessor. The resulting processed NSU3D grid is then used within CREATE-AV KESTREL and FUN3D for consistency. For CREATE-AV KESTREL this grid is converted to AVMesh format using the CREATE-AV KESTREL preprocessor, FUN3D is able to read in the NSU3D file format with no modification. Some CREATE-AV HELIOS cases were run with an unstructured near-body and a Cartesian off-body. This grid (Grid-5) contains a constant cell size with trim distances ranging from 0.25 inches to 0.5 inches. The first set of cases run use the ROBIN-mod7 fuselage with a pylon on the top as shown in Figure 2. The wind tunnel model has this removed in order to add the mount. The corresponding "free-air" OVERFLOW predictions were run without this pylon. Thus, a second series of cases were run for each solver using the model with no pylon. The boundary layer spacing in all cases is selected to ensure that the y^+ value is less than one over the entire fuselage.

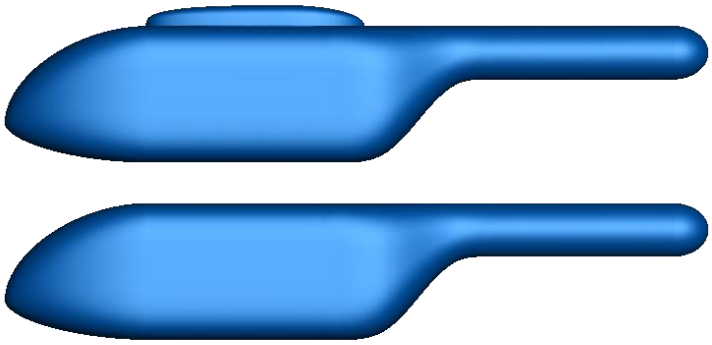

Figure 2. Surfaces used in the CFD grids with and without the pylon.

Table 1. Grids used during study.

	Boundary Layer Cells	# of Cells	# of Nodes	Description
Grid 1	Prisms	8.7M	2.3M	Coarse grid case
Grid 2	Tetrahedra	24.0M	4.1M	Refined grid case
Grid 2	Prisms	14.0M	4.1M	Refined grid case
Grid 5	Prisms	15.5M	5.5M	0.05" cell size, HELIOS dual mesh only
Grid 6	Prisms	22.3M	5.3M	No pylon, additional aft refinement

V. Results

All solutions were run using the Spalart-Allmaras turbulence model in order to compare more directly with the available OVERFLOW data. This section looks at grid resolution and the impact of equation modifications before performing any direct solver comparisons. It is important to note that the presence of the wind tunnel walls and model mount do have an impact on the measured data. The CFD solutions presented here do not model the wind tunnel walls or the mount. It was demonstrated that modeling the wind tunnel walls and mount is necessary in order to match the test data in Reference 1. This comparison ran OVERFLOW with and without the tunnel modeled and compared the solutions. The results with the tunnel are much closer to the experimental data than the results without these features. Thus, a better comparison for the present study is achieved by using the OVERFLOW data computed in "free-air" as the baseline.

A. Grid Independence Study

Grid-1, Grid-2, and Grid-5 were used to assess grid independence. Grid-5 does not have sufficiently far outer boundaries and was designed specifically for the CREATE-AV HELIOS dual mesh capability. Figure 3 compares CREATE-AV KESTREL solutions using Grid-1 and Grid-2. The data are nearly identical confirming that approximate grid independence has been achieved for this case.

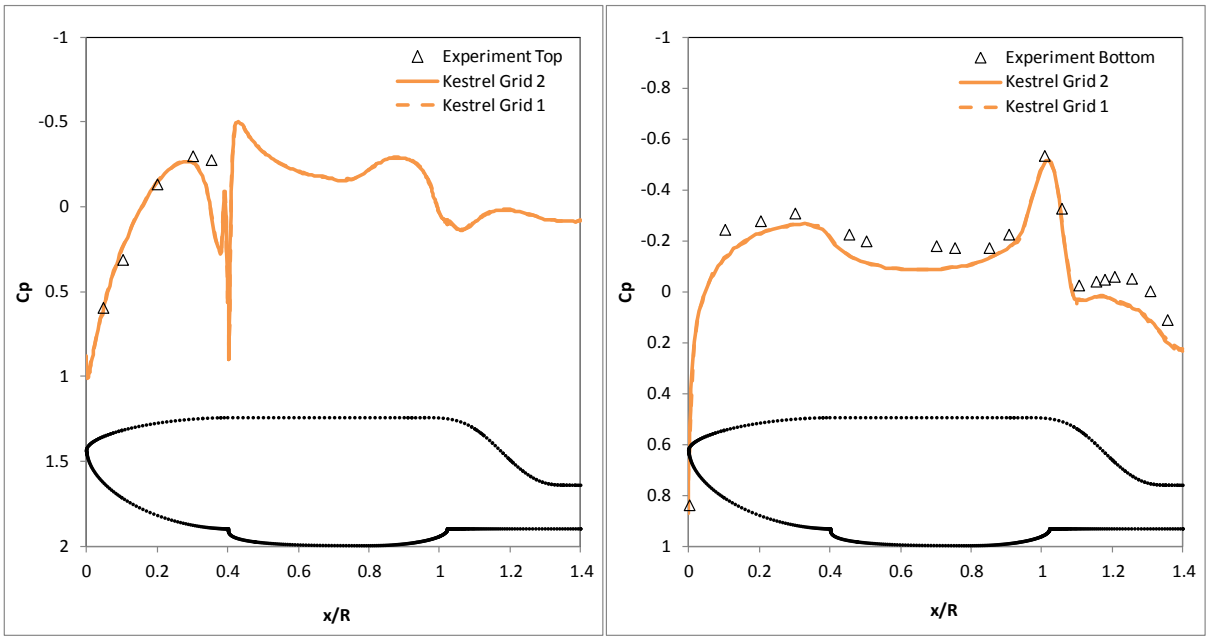

Figure 3. Grid independence for CREATE-AV KESTREL solutions.

The CREATE-AV HELIOS grid comparisons are shown in Figure 4. The solutions reveal that for Grid-1 and Grid-2 the solutions are nearly identical. This is also true of Grid-5 in the attached flow regions. However, there is a large difference in the separated region when employing the dual mesh methodology with Grid-5. This is hypothesized to be the result of having a finer off-body mesh in the region aft of the fuselage in the separated flow region as well as having higher order spatial accuracy in the off-body solver. This hypothesis was partially tested by creating an unstructured mesh (Grid-6) with additional refinement in the same aft region and running an isolated NSU3D case on this mesh. The results do show some improvement in the separated region with the additional refinement. It should be noted that the dual mesh case is not using the isolated NSU3D solver as is used for Grid-1 and Grid-2. The Grid-5 case uses a combined NSU3D/ARC3D solver where the ARC3D solver is applying the Euler equations in the off-body.

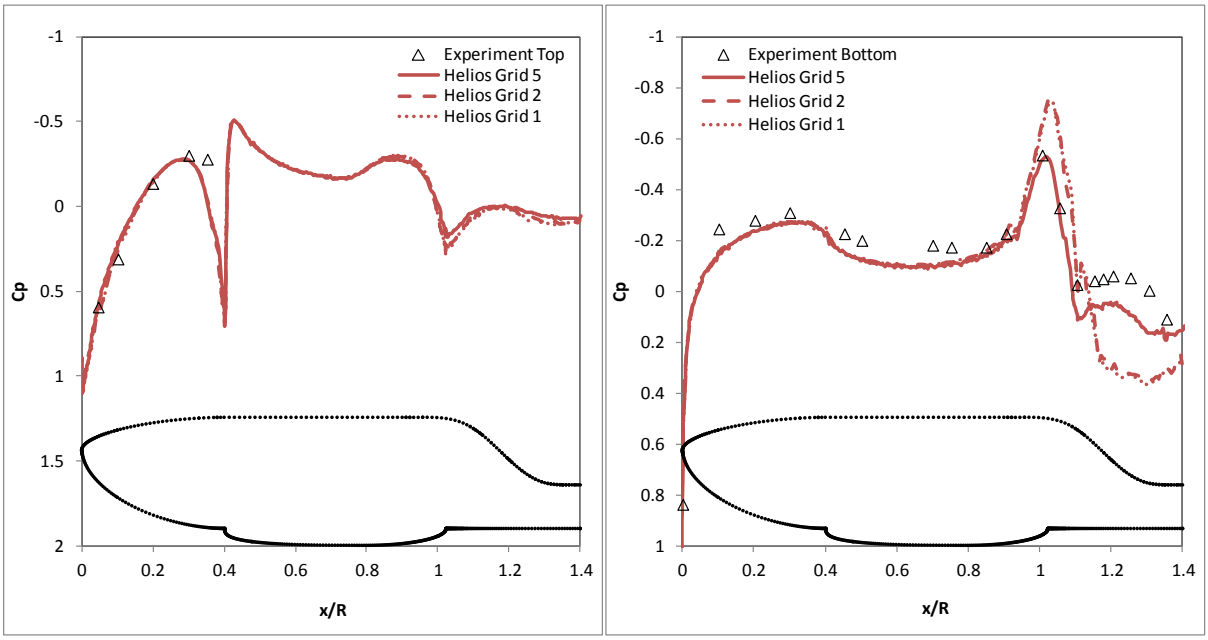

Figure 4. Grid independence for CREATE-AV HELIOS solutions.

B. Tetrahedral vs. Prismatic Boundary Layers

All the grids developed for this study use no-slip boundary conditions for the fuselage surfaces. This boundary condition requires the presence of sufficient grid cells close to the surface in order to resolve the boundary layer flow gradients. This is accomplished by layering high aspect ratio cells near the fuselage surfaces. These are often called viscous layers. The grid generation software used for this study only generates tetrahedral cells. In these cases, it is common practice to employ preprocessing software to convert the tetrahedral cell structure within the viscous layers into a prismatic cell structure by combining, or merging, the tetrahedral cells. Solutions using the unmerged viscous layer grids were computed using both CREATE-AV KESTREL and FUN3D. These solutions are compared to the corresponding merged viscous layer grid solutions in Figure 5. Over the top of the fuselage there is little difference between the four solutions. The structure of the boundary layer mesh starts to have an impact aft of the pylon where there is a small region of flow separation. Over the bottom of the fuselage the boundary layer mesh structure again has little impact over the front portion of the fuselage. However, in the region of separation there is a noticeable difference between the solutions. This impact appears to be more significant for CREATE-AV KESTREL than for FUN3D and may have to do with differences between the node-centered and cell-centered methodologies. In general, the difference between the merged and the tetrahedral boundary layers is that the prismatic cell faces are aligned perpendicular or normal to the surface whereas the tetrahedrons have faces that are not all aligned with the surface. This impacts the computations in the boundary layer.

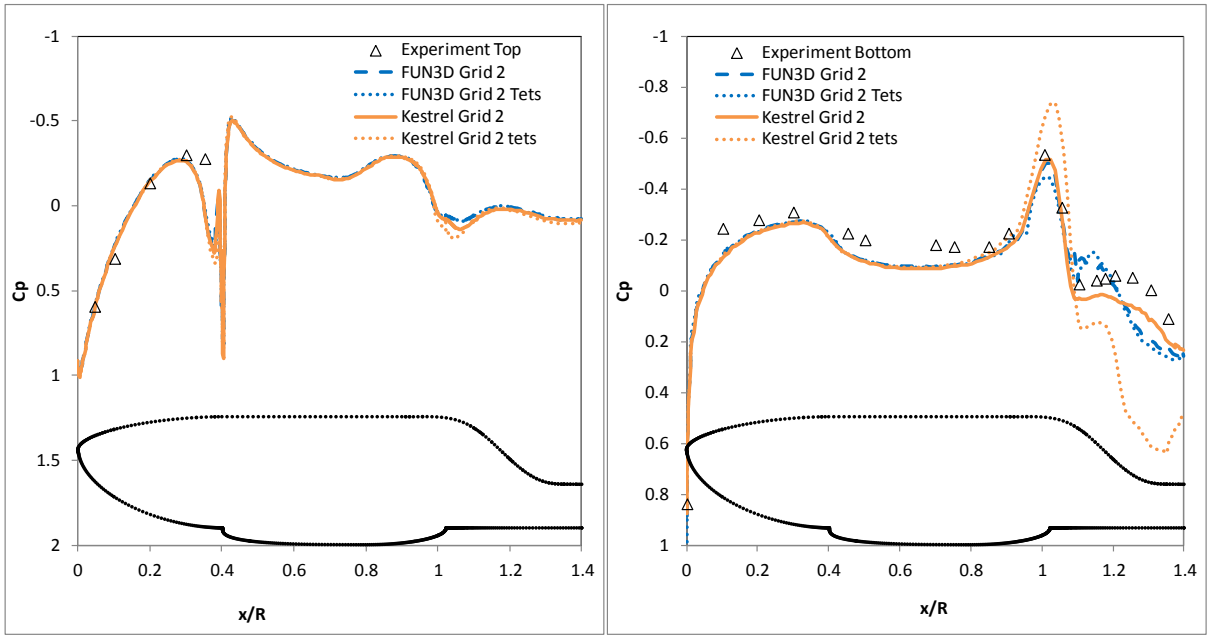

Figure 5. Centerline pressures comparing tetrahedral vs. prismatic boundary layers.

C. Compressible vs. Incompressible Solvers

FUN3D has the option to run either the compressible or the incompressible Navier-Stokes equations. These two methods are compared in Figure 6. For the incompressible solution an artificial compressibility factor of 10.0 is used. In the attached flow regions the solutions are identical. However, in the separated flow region the compressible solution displays higher frequency fluctuations near the separation point while the incompressible solution is much smoother and more closely follows the test data. This is not surprising since the compressible equations can suffer from high equation stiffness in low Mach flows and as a result predict non-physical numerical fluctuations in the solution. Typically, either a low Mach preconditioning method or switching to the incompressible Navier-Stokes equations is employed to alleviate the stiffness problem. In this case, the numerical fluctuations are directly impacting the separation region and thus the downstream predictions from this point.

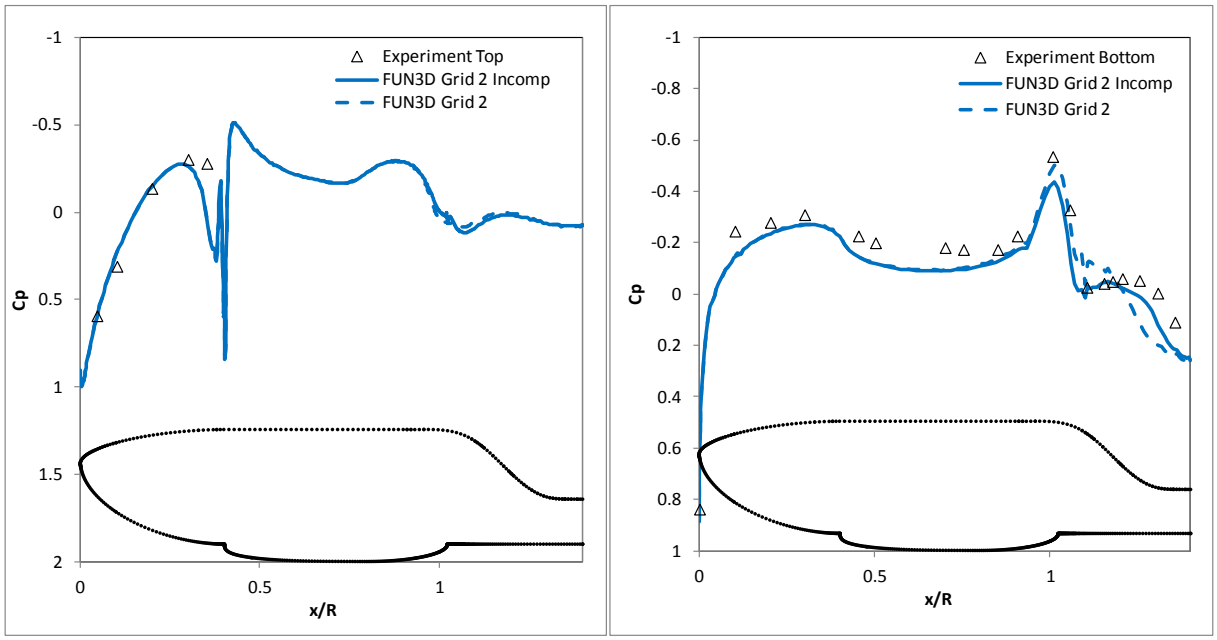

Figure 6. Centerline pressures comparing compressible and incompressible solutions in FUN3D.

A low Mach number preconditioning option is available in CREATE-AV HELIOS and was pursued as part of this study. These cases investigated changes to the β_{min} parameter. However, converged cases were not obtainable and thus will not be presented here.

D. Comparison of Near-Body Trim Distance in HELIOS Dual Mesh Cases

The dual mesh feature in CREATE-AV HELIOS employs a near-body unstructured mesh surrounded by a Cartesian off-body mesh. The position of the overlapping region between these meshes is adjusted by trimming the near-body mesh to a fixed distance from the solid surfaces. This method cuts away near-body cells that lie beyond the user defined trim distance before the off-body mesh is generated. A set of cases was run to evaluate the impact of the near-body trim distance on the solution. This case is set-up specifically so that the only variable that changes is the position of the near-body and off-body mesh fringes. This was accomplished by generating a near-body grid with a constant cell size throughout the mesh (Grid-5). The exception to this constant cell size is the viscous grid layering which use the same surface normal size distribution as the single mesh cases. Around this near-body mesh is a fixed off-body Cartesian mesh with the same constant cell size that is set in the near-body. The near-body mesh trim distances applied are 0.25 in, 0.3 in, 0.35 in, and 0.5 in. A sample slice through the 0.3 in mesh is provided in Figure 7.

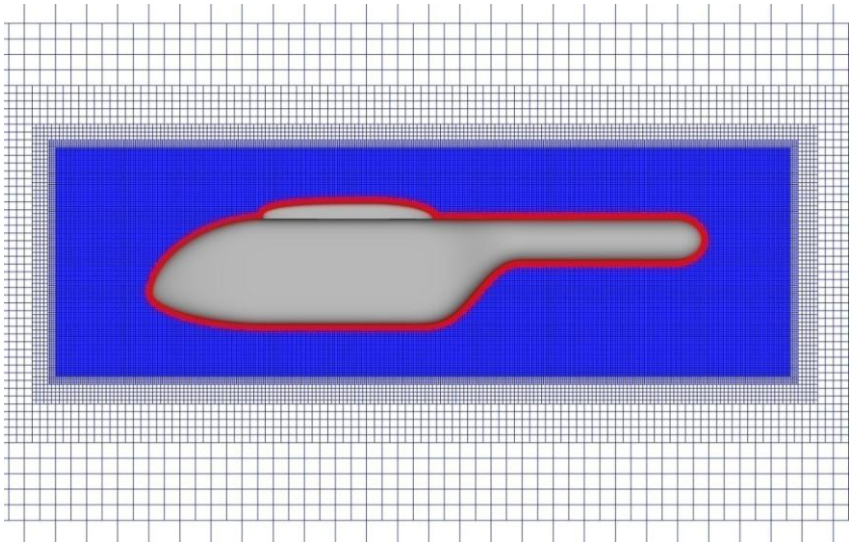

Figure 7. Grid slice through the dual mesh for the 0.3 in trim case (red = near-body, blue = off-body).

There are two considerations when selecting a near-body trim distance; geometric and solution based. The geometric issues involve the quality of the fringes supplied to PUNDIT to overset the near-body and off-body meshes. The solution based issues involve making sure that

the Euler off-body solution does not cover any regions where viscous effects are important. The consequences of exceeding the geometric limit are best shown in the 0.25 in trim case. This case computed a total of 4515 orphans. These orphans are illustrated in Figure 8 where the orphan locations are represented by the green spots. All of these orphans are located in places where the off-body Cartesian mesh intersects the second viscous grid layer. In this plot the black represents the off-body mesh, the red and blue represent the near-body mesh where the blue is the near-body fringe. Therefore, the trim distance must be increased in order to move the off-body fringe away from the viscous grid layers and thus reduce the number of orphans. The 0.3 in case has a total of 241 orphans. This is below the default reject threshold of 1000 and was allowed to complete. The 0.35 in and the 0.5 in cases both compute zero orphans.

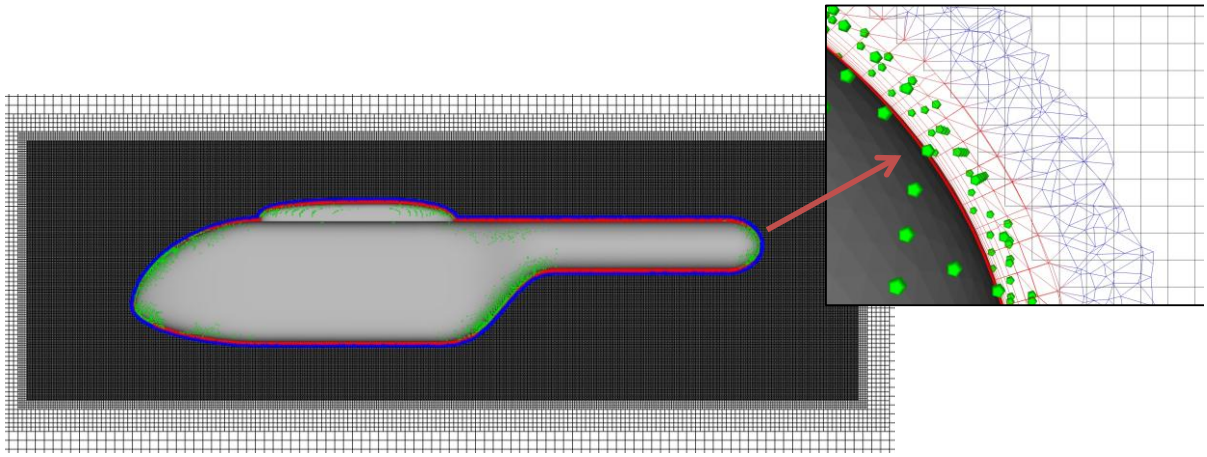

Figure 8. Orphan locations for the 0.25 in trim distance case.

The next step is to make sure that the Euler solution does not overlap the viscous regions. This is more difficult to identify, but generally requires that the off-body not cut into the boundary layer. The centerline pressure predictions for the 0.3 in, 0.35 in, and the 0.5 in trim cases are compared in Figure 9. It is apparent from this comparison that the Euler assumptions in the off-body are interfering with the near-body predictions in the 0.3 in case. This is further illustrated in Figure 10 where there is additional unsteadiness predicted around the attached flow regions of the fuselage. The solutions for the 0.35 in and the 0.5 in cases are much smoother and predict the same solution for the attached flow regions. Thus, in these regions the Euler off-body is not overlapping the

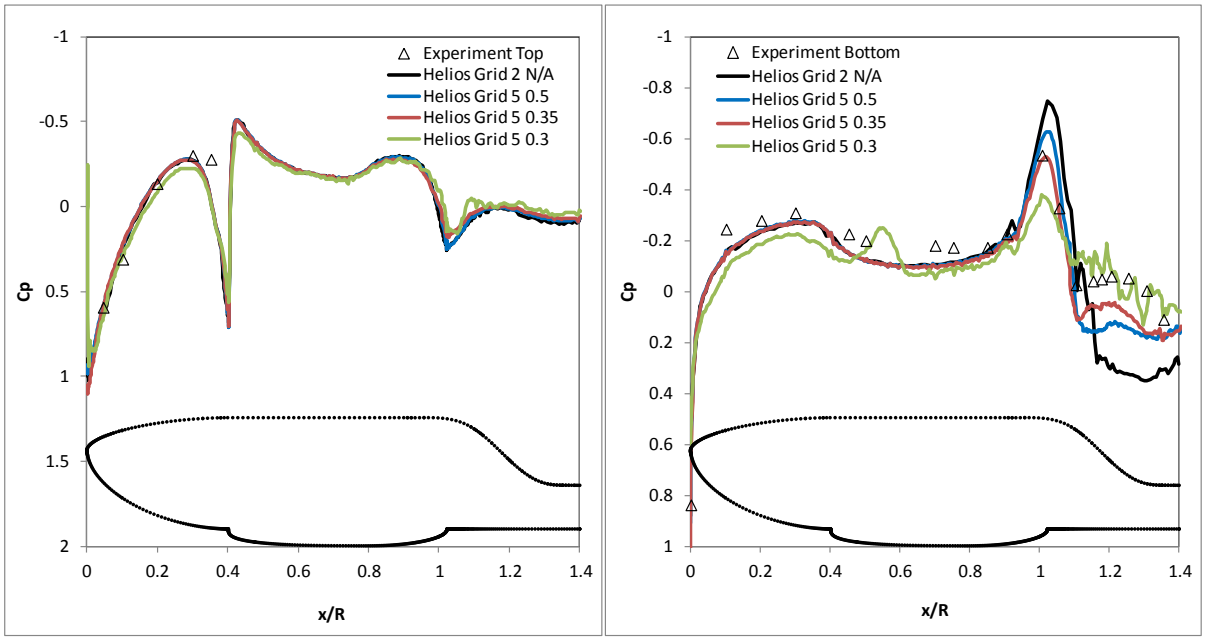

Figure 9. Centerline pressures comparing near-body trim distance in Helios dual mesh cases.

boundary layer for trim distances greater than 0.35 in.

In the separated flow region, the solutions begin to diverge. The single mesh case is included to show that as the trim distance is increased the solution is trending towards the single mesh case. However, the equivalent single mesh case would actually use a much finer grid than the Grid-2 case plotted here. There seems to be an optimum point between 0.3 in and 0.35 in that would produce the closest solution. However, a solution dependent on trim distance is not the ideal situation. The off-body mesh is intended to provide both efficiency and accuracy to the solution through quicker per node computation time, increased spatial order of accuracy, and adaptive mesh refinement. In this case, for which the mesh refinement is fixed, the variables that differ between the near-body and the off-body are primarily the inviscid flow assumption and the increased spatial accuracy. The spatial accuracy would certainly increase the resolution of the flow structures in the flow aft of the fuselage in the off-body region. It may be that the increased spatial order of accuracy close to the surface is impacting the separation characteristics, or it may be that the trim distance is not sufficiently large in the separated flow region so that the Euler flow assumption is valid.

E. Initial Solver Comparison

This initial solver comparison looks specifically at comparing the best solutions obtained with each solver using the geometry with the pylon included. For CREATE-AV KESTREL this is the Grid-2 merged boundary layer case, for FUN3D this is the Grid-2 merged boundary layer incompressible case, and for CREATE-AV HELIOS this is the Grid-5 combined NSU3D/ARC3D solution with the additional off-body refinement aft of the fuselage and the 0.35 in trim distance. The isolated NSU3D solution using Grid-2 is included since it matches the FUN3D and CREATE-AV KESTREL conditions the closest. These solutions are plotted in Figure 11. For the attached flow region the solutions are almost identical, there is a small divergence for the NSU3D solution along the bottom of the fuselage. In the separated flow regions each code predicts a different solution. The CREATE-AV HELIOS dual mesh and CREATE-AV KESTREL solutions seem to predict the peak the best, while FUN3D seems to predict the separation point the best. The isolated NSU3D solution has the greatest error. It should be noted that since the wind tunnel walls are not modeled here that it is unknown exactly how far off the free air predictions should be from the measured data. The next section that compares the OVERFLOW data with the current predictions will approximate this delta.

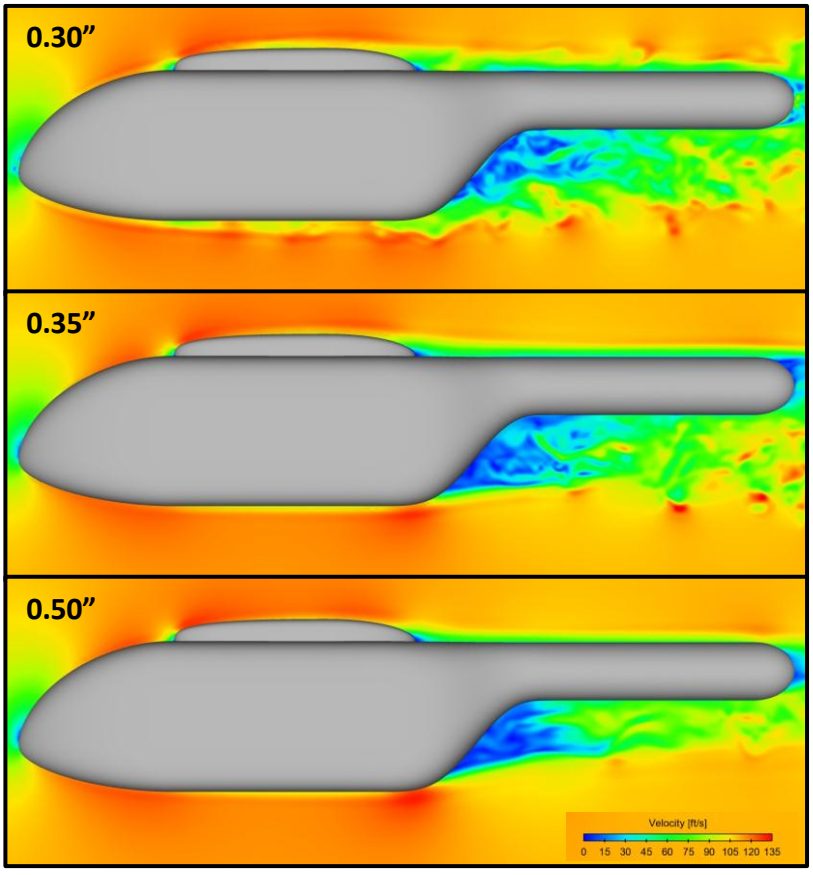

Figure 10. Centerline slices comparing the velocity contours for different near-body trim distances.

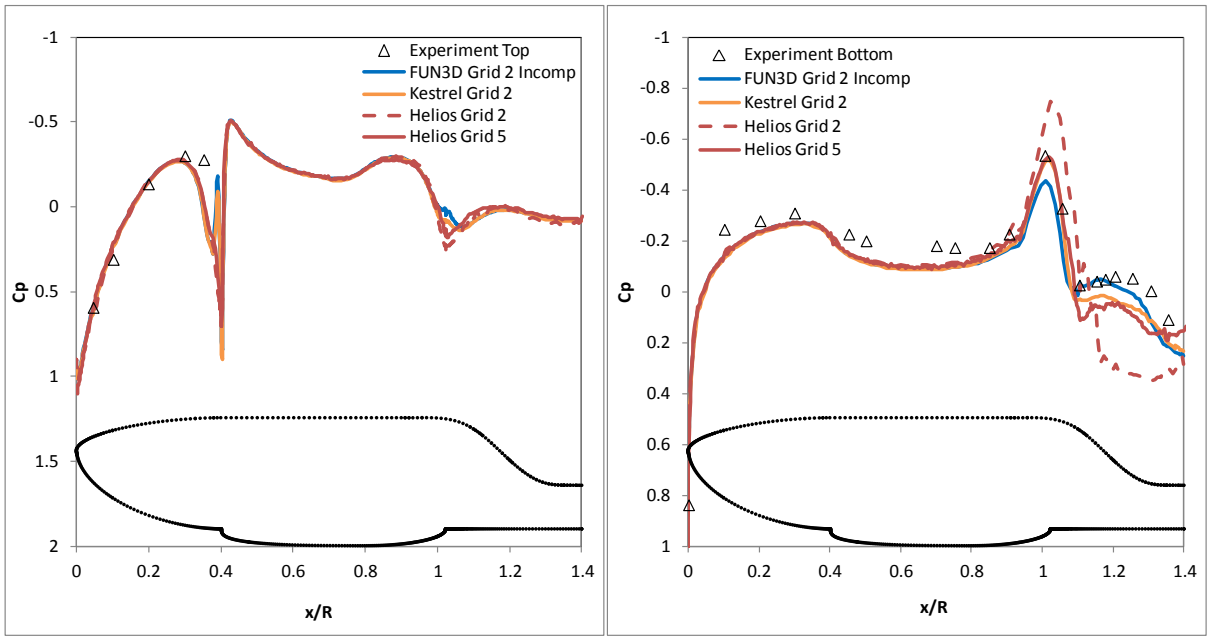

Figure 11. Centerline pressures comparing the best solutions for the model with the pylon included.

The comparison of the oil line plots with the test data in Figure 12 reveal somewhat different conclusions. In these plots, FUN3D and CREATE-AV HELIOS dual mesh predict the separation point the closest, while CREATE-AV KESTREL and NSU3D are separating later. The red circles indicate the experimental separation point.

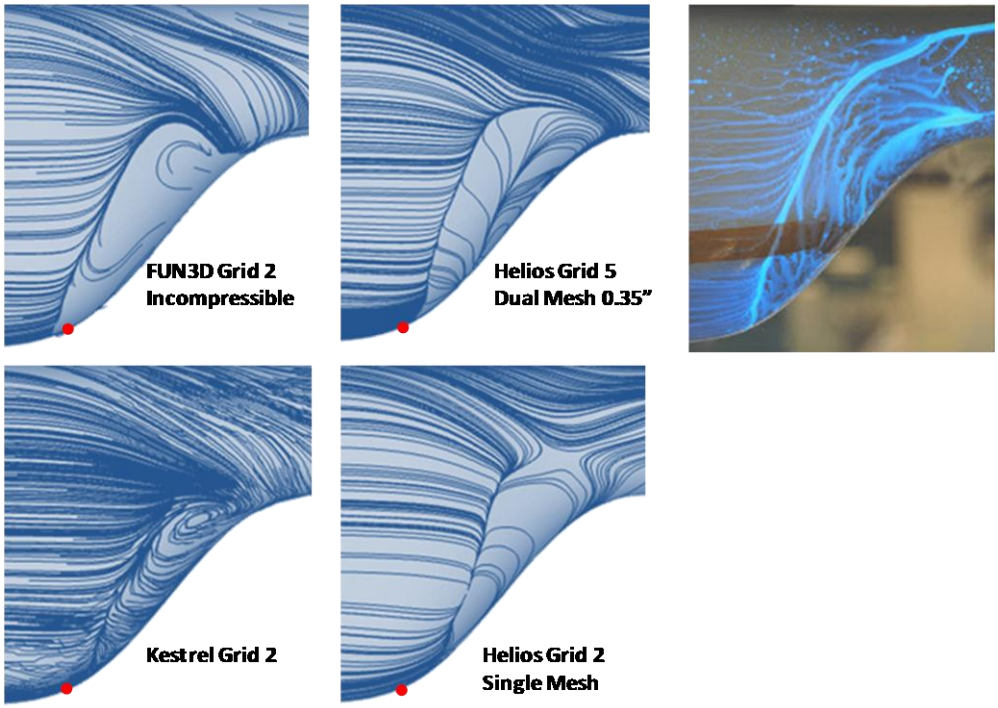

Figure 12. Oil line plots comparing flow separation points against experiment.

The integrated drag listed in Table 2 indicates that each code is predicting a somewhat different drag coefficient. This is true of both the viscous and the pressure drag components. It should be noted that the experimental value is expected to be higher than the computed values since the tunnel walls are not present in the CFD solutions.

Table 2. Integrated drag subdivided into viscous and pressure components.

	Drag Coefficient	Viscous Drag Coefficient	Pressure Drag Coefficient
Experiment	0.145		
KESTREL Grid-2	0.114	0.059	0.055
HELIOS Grid-5 (Dual Mesh)	0.088	0.044	0.044
HELIOS Grid-2	0.086	0.050	0.036
FUN3D Grid-2 (Incomp)	0.129	0.056	0.073

F. Final Solver Comparison

This final comparison provides the opportunity to compare the three current solvers against the OVERFLOW data, since the same geometry with the pylon removed is used for all of these cases. The best solution for each code is compared in this section. For CREATE-AV HELIOS and for CREATE-AV KESTREL these are the standard compressible case, and for FUN3D this is the incompressible case.

Table 3. Integrated drag separated into pressure and viscous components (%error compared to OVERFLOW free-air results).

	Drag Coefficient	Viscous Drag Coefficient	Pressure Drag Coefficient	Percent Error
Experiment	0.145			
OVERFLOW (Tunnel)	0.145	0.055	0.090	
OVERFLOW (Free-air)	0.114	0.056	0.058	
HELIOS Grid-6	0.082	0.049	0.034	-27.7%
KESTREL Grid-6	0.108	0.057	0.051	-5.49%
FUN3D Grid-6 (Incomp)	0.120	0.053	0.067	5.56%

Table 3 lists the integrated drag for each code. In this table the OVERFLOW solutions include a version with the tunnel walls modeled and a version that does not include the tunnel walls in the model. The tunnel solution is expected to match the experimental data the closest, and in fact the drag coefficients are the same, while the free-air solution is used to represent the expected delta between the experimental data and the remaining CFD solutions. Thus, the percent errors listed in the last column are computed against the OVERFLOW free-air data. Each of the three solvers predicts a different integrate drag. Both CREATE-AV HELIOS and CREATE-AV KESTREL are underpredicting the drag coefficient, but to different degrees. Both codes seem to be underpredicting the pressure drag when compared with the OVERFLOW data, while CREATE-AV KESTREL is the closest to the viscous drag. FUN3D is overpredicting the drag, where the viscous drag is lower than the OVERFLOW free-air data while the pressure drag is much higher. The viscous drag is dependent on the gradients close to the surface, while the pressure drag is going to vary depending on the separation point aft of the fuselage. Looking at

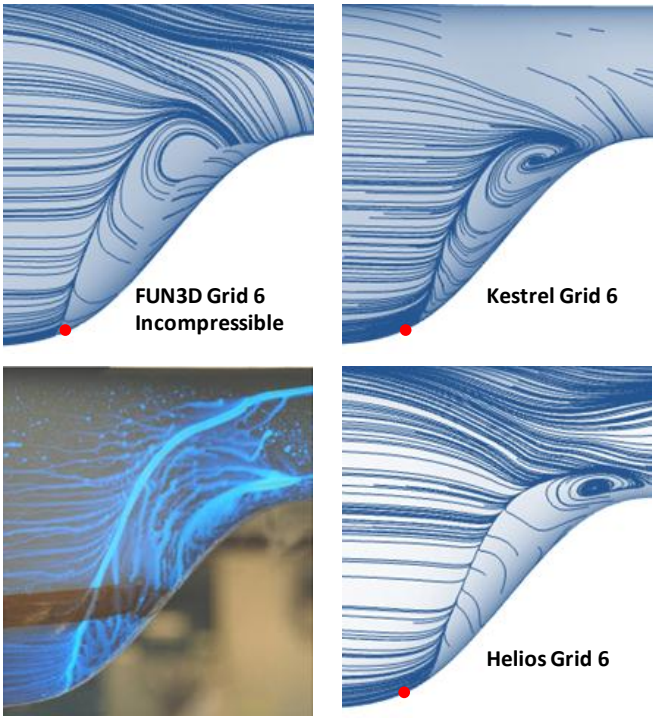

Figure 13. Oil line plots comparing flow separation points against experiment for Grid-6.

the distributed predictions will clarify the differences seen in the table.

Figure 13 plots the oil line plots in the separation region aft of the fuselage for CREATE-AV HELIOS, CREATE-AV KESTREL, and FUN3D compared to the tunnel data. The separation point in FUN3D is the earliest and corresponds with the higher pressure drag seen in the table. The CREATE-AV KESTREL separation point is next followed by the CREATE-AV HELIOS separation point. The corresponding pressure drag components also follow this trend. The increased grid density aft of the fuselage is having a positive effect on the solution compared to the Grid-2 cases plotted in the previous section. The centerline slice contours are plotted in Figure 14 for comparison. These plots indicate that the three codes have similar, but not identical separated flow characteristics. The integrated pressure drag indicates that the OVERFLOW solution separates after FUN3D, but before CREATE-AV HELIOS and CREATE-AV KESTREL. The separation data are not available to confirm this, but the pressure tap data are available for comparison.

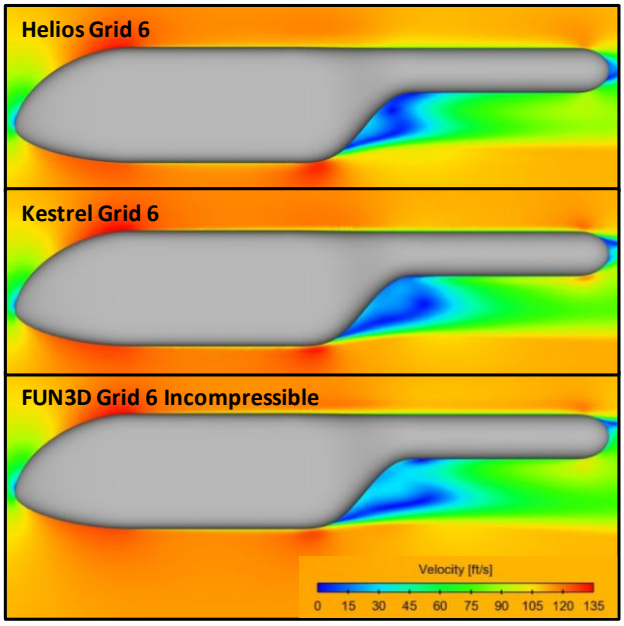

Figure 14. Centerline slices comparing the velocity contours.

The centerline pressures plotted in Figure 15 also include the OVERFLOW data with and without the tunnel walls. The OVERFLOW solution with the tunnel walls matches the experimental data the closest. When these walls are removed the magnitude of the pressure coefficient drops. All of the CFD solutions without the tunnel walls match in the attached flow regions along the top of the fuselage and along the bottom for the front half of the fuselage. In the separated region the solutions begin to diverge. The general trends are the same, but the magnitudes are different. CREATE-AV KESTREL matches the OVERFLOW data the closest. FUN3D matches the test data after the separation point the closest. The CREATE-AV HELIOS (NSU3D) data are the farthest from the predictions. A matching dual mesh case was not run without the pylon, but based on earlier results it is expected that this would improve the CREATE-AV HELIOS prediction.

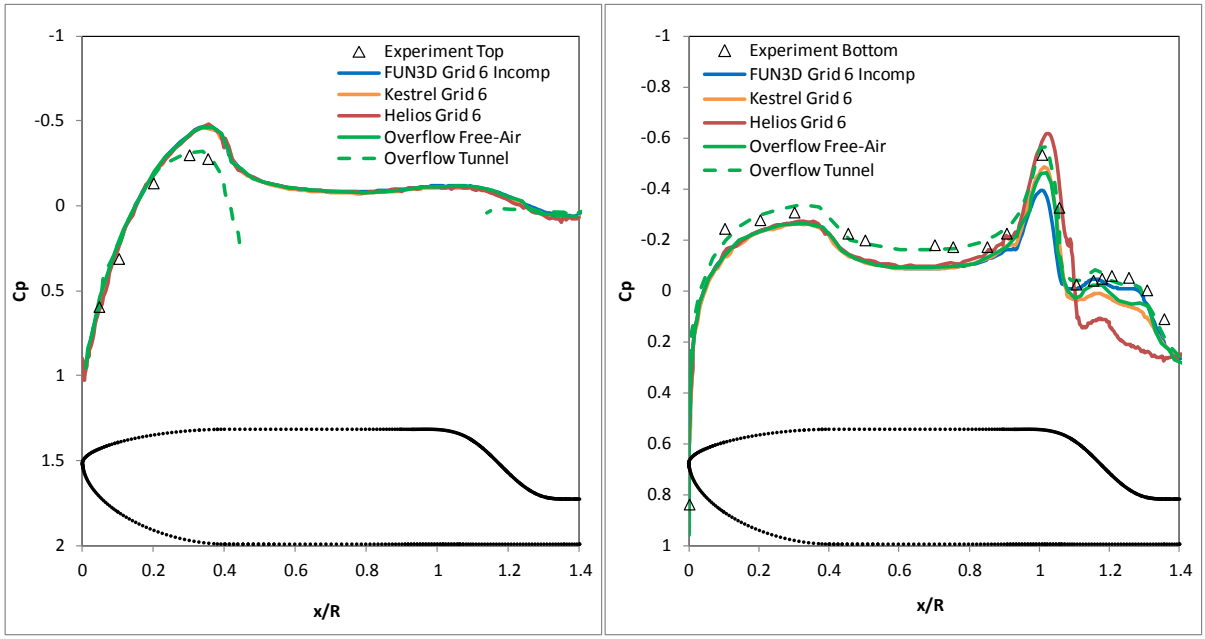

Figure 15. Centerline pressures comparing the best solutions for the model with the pylon removed.

Overall, the best solutions from all four CFD codes are consistent with one another except for the separated flow region where the character of the solutions are the same, but the magnitudes differ. These differing magnitudes in the predicted results are impacting the integrated drag. Overall, the isolated NSU3D results are not performing as well as the isolated kCFD results.

G. Computational Metrics

The computational metrics give a good idea of how fast each code is able to run. However, the timing alone does not always give the full picture. This section compares both the computational time used as well as the solution convergence characteristics to provide a full picture of how fast a solution may be expected to complete.

1) Timing Comparison

All cases presented here were run on Spirit. Spirit is an SGI ICEX machine running on Intel E5 Sandy Bridge 2.6 GHz processors with 16 cores per node and 32Gb per node. Some variability in the run time is detected when the timing of similar restart cases is compared. Thus, the timing comparisons provided in Table 4 cannot be considered absolute, but do allow for general code to code comparisons. The times listed in the table also include all of the pre- and post-processing steps included in the case. This was done for consistency since internal time per iteration values are not available for all codes. Instead the total time for each case is used in the table. When comparing the results, the CREATE-AV HELIOS dual mesh methodology runs the fastest in terms of the time per processor per iteration per degree of freedom. This is followed by NSU3D then CREATE-AV KESTREL, with FUN3D as the slowest of the codes.

Table 4. Computational timing comparisons.

Code(s) Run	Grid	Degrees of Freedom	Procs	Wall Clock [hrs]	Iterations	Time/proc/it/DoF [nanosec]
HELIOS (NSU3D & ARC3D)	Grid-5	55M (nodes near) 91M (nodes off)	512	2.77	10K	0.0203
HELIOS (NSU3D)	Grid-2	4.1M nodes	512	1.95	50K	0.0673
KESTREL	Grid-2	14.0M cells	512	24.39	50K	0.2441
FUN3D (Incompressible)	Grid-2	4.1M nodes	256	5.19	30K	0.5971

2) Convergence Comparison

The convergence characteristics tell the opposite story. Figure 16 compares plots of the drag coefficient convergence for each of the cases listed in Table 4. In these plots FUN3D converges the fastest followed by CREATE-AV KESTREL then CREATE-AV HELIOS dual mesh with NSU3D as the slowest to converge. The x-axis of each of these plots represents the total iterations that the code was run for each of these cases. The isolated NSU3D case ran up to one million iterations. This case was run past this point, by renumbering the restart directory to a smaller iteration number, but because of internal formatting limits the iterations beyond one million were not saved. The CREATE-AV HELIOS dual mesh case did not reach a single steady-state value because the mesh behind the fuselage is much finer than for the Grid-2 cases. Thus, the refinement of the unsteady flow in this region prevents the solution from reaching a single value. The FUN3D and CREATE-AV KESTREL cases converged fairly quickly and were run well past the minimum convergence point.

In order to get a better idea of how long a user would expect to wait for a solution to complete, the minimum convergence points are identified and extracted from the convergence plots. Obtaining a solution overnight is used as the ideal situation; this represents a wall time of less than 12 hours. The minimum convergence points are identified using the drag convergence only. In reality, the moments take longer to converge, but the drag convergence may be used for comparison purposes. These minimum values are listed in Table 5. By extracting the time per iteration from the previous table and multiplying by the minimum required iterations, a minimum total wall clock time may be estimated. This wall time represents how long a user would have to wait to obtain a completed solution.

Comparing these values reveals an interesting reversal. Even though CREATE-AV HELIOS runs the fastest, it converges the slowest, requiring many more iterations to complete. Thus, the wall clock time does not allow for

obtaining a solution overnight under the test conditions. It should be noted that NSU3D does have a multi-grid option which should improve the convergence, but this option was not attempted during this study. CREATE-AV KESTREL and FUN3D both converge much faster allowing for the possibility of obtaining a solution overnight even though the codes do not run as fast as CREATE-AV HELIOS.

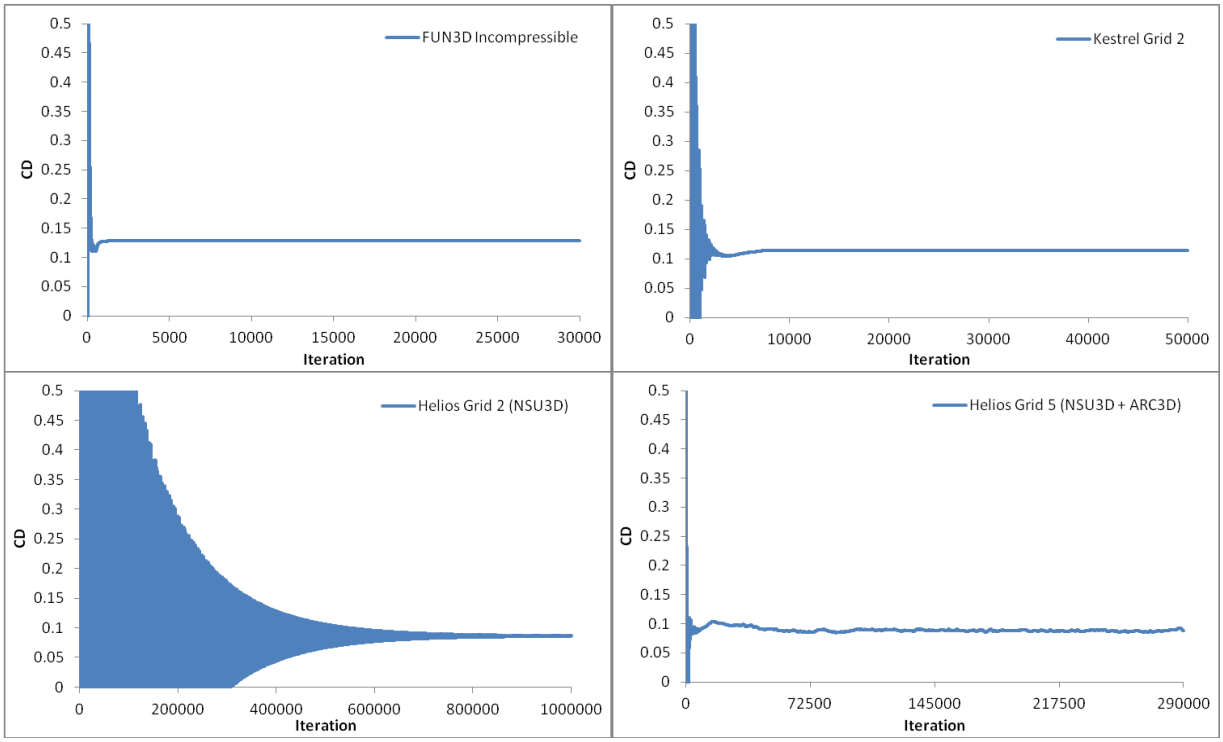

Figure 16. Drag coefficient convergence comparison for selected cases (x-axis maximum represents total iterations run).

Table 5. Estimated computational timing comparisons.

Code(s) Run	Grid	Degrees of Freedom	Estimated iterations to converge	Procs	Estimated Wall Time [hrs]
HELIOS (NSU3D & ARC3D)	Grid-5	5.5M (nodes near) 91M (nodes off)	100K	512	27.70
HELIOS (NSU3D)	Grid-2	4.1M nodes	1M	512	39.00
KESTREL	Grid-2	14.0M cells	9K	512	4.39
FUN3D (Incompressible)	Grid-2	4.1M nodes	2.5K	256	0.43

VI. Conclusion

A study of three locally available CFD solvers (HPCMP CREATE™-AV HELIOS, HPCMP CREATE™-AV KESTREL, and FUN3D) are compared against both experimental and OVERFLOW data obtained from reference 1. These three solvers are compared using variations in the grid and solver parameters. The conclusions from this study include,

- Grid independence studies comparing Grid-1 and Grid-2 in both CREATE-AV KESTREL and CREATE-AV HELIOS indicate that grid independence has been reached in both solvers.

- The comparison of tetrahedral vs. prismatic boundary layers indicates that the surface aligned faces in the prismatic boundary layer yield better results than the unaligned faces in the tetrahedral boundary layer. This difference is stronger in the cell-centered CREATE-AV KESTREL code than in the node-centered FUN3D code.
- The use of the incompressible equations reduces the incidence of non-physical numerical fluctuation in the FUN3D solution.
- When setting up a dual mesh case in CREATE-AV HELIOS care must be taken when defining the fringe distance to both create a proper fringe for the oversetting process, as well as to keep sufficient distance of the off-body solver from the viscous flow regions.
- The initial comparison with the pylon included indicate that in the attached flow regions all of the solutions predict approximately the same results. The separated regions predict different magnitude solutions with the isolated NSU3D solution being the furthest from the experimental data.
- The final comparison with the pylon removed allows for the comparison with the OVERFLOW data. In this comparison all of the local CFD solvers predicted the drag to be within 6% error with the exception of the CREATE-AV HELIOS prediction. The distributed data showed that the differences are primarily in the separated flow aft of the fuselage.
- The computational metrics show that CREATE-AV HELIOS runs the fastest and CREATE-AV KESTREL and FUN3D run the slowest. However, the increased rate of convergence in CREATE-AV KESTREL and FUN3D allow for a solution to be obtained overnight, while more time is needed for a CREATE-AV HELIOS solution.

Finally, it should be pointed out that this study did not do a thorough investigation of optimal solver settings, default settings in the solvers were used in most cases, only a few deviations from these settings were attempted. Since HELIOS is applied primarily to rotor-based flows, as opposed to isolated fuselages like the fixed-wing kCFD code, the default settings in HELIOS may not have been ideal for this fuselage case. Future work will investigate alternative solver settings in HELIOS in order to see if the results improve.

Acknowledgments

The authors would like to acknowledge the support of the HPCMP CREATE™-AV Program and the supercomputing resources provided by the HPCMP, in particular the Air Force Research Lab (AFRL). The contribution of Rajneesh Singh of providing the original ROBIN surface mesh is also gratefully acknowledged.

References

[1]Schaeffler, N. W., Allan, B. G., Lienard, C., and Le Pape, A., "Progress Towards Fuselage Drag Reduction via Active Flow Control: A Combined CFD and Experimental Effort," *36th European Rotorcraft Forum*, Paris, France, September 7-9, 2010.

[2]Singh, R., and Dinavahi, S., "Aerodynamic Force Computations for Rotorcraft Fuselage," *50th AIAA Aerospace Sciences Meeting*, Nashville, TN, January 9-12, 2012.

[3]HPCMP CREATE™-AV On-line Resources, "https://portal.create.hpc.mil/authdocs/av/index.php," Last Accessed November 18th, 2013.

[4]FUN3D On-line Resources, "http://fun3d.larc.nasa.gov," Last Accessed November 18th, 2013.